were low (that is, fewer Coulomb collisions) in the torus (*12, 13*). Alternatively, the spatial relation between the cool and hot components of the plasma torus and Io's sodium cloud might have changed. As a result, more neutral particles would encounter hot ions. Table 1 summarizes the full set of observational and model-derived quantities.

The three-dimensional distribution of the Na* volume density required to match an image can be modeled within the charge-exchange framework discussed above (*4, 5*) (Fig. 2). The Ulysses trajectory through the modeled particle distribution can be used to specify the [Na*] density at the spacecraft's location (Fig. 3). For simulation runs with and without photo-ionization, there is a slight difference between the [Na*] distributions; these are designated [Na^+] in Fig. 3. It should be noted that Na^+ can appear by other means (*14*). Moreover, the Na^+ energy should be higher than the 600 eV associated with corotational escape from Io's location because of capture by the rapidly rotating magnetic field at larger distances. Nevertheless, the simulations depicted in Fig. 3 should give a good prediction for fast neutral clouds (Na* is a tracer for other gases). In the absence of significant radial transport, the simulations also provide a rough estimate of where ions produced by solar EUV might appear. Scaling of this latter effect to gases other than sodium would require the use of their respective solar ionizing time constants in the simulation.

In summary, ground-based imaging observations of Jupiter's great sodium nebula during the Ulysses encounter period indicated that (i) volcanic activity on Io preceding the Ulysses encounter must have been lower than observed in 1989 to 1990; (ii) plasma torus densities derived from the neutrals were proportionally lower; and (iii) the ion thermal structure in the torus was higher than in previous years.

REFERENCES AND NOTES

1. M. Mendillo *et al.*, *Nature* **348**, 312 (1990).
2. A. Eviatar, Y. Mekler, and F. V. Coroniti [*Astrophys. J.* **205**, 662 (1976)] predicted a flux of hot (fast) neutral sodium that was subsequently observed and treated in detail by R. Brown and N. Schneider [*Icarus* **48**, 519 (1981)].
3. N. M. Schneider *et al.*, *Science* **253**, 1394 (1991).
4. W. Smyth and M. Combi, *J. Geophys. Res.* **96**, 22711 (1991).
5. B. Flynn, M. Mendillo, J. Baumgardner, *Icarus*, in press.
6. N. Schneider, W. Smyth, M. McGrath, in *Time-Variable Phenomena in the Jovian System*, M. Belton, R. West, J. Rahe, Eds. [National Aeronautics and Space Administration (NASA), Washington, DC, 1989], pp. 75–94.
7. Io is located at 5.9 R_J, where the orbital speed is 17.3 km/s. The corotation speed at 5.9 R_J is 74 km/s.
8. The dominant ion species in the plasma torus are O^+, S^+, and S^{2+}. See review by F. Bagenal, in *Time-Variable Phenomena in the Jovian System*, M. Belton, R. West, J. Rahe, Eds. (NASA, Washington, DC, 1989), pp. 196–210.
9. N. Schneider, *Eos* **73**, 173 (1992).
10. With the approximations that all Na* is confined within the flaring angle and that the nebula is azimuthally symmetric, the source rate becomes $S(Na^*) = 4\pi r^2 \sin\theta\, V_{term} n$, where r is the distance from Jupiter, θ is the flaring angle, V_{term} is the terminal flow speed (70 km/s), and $n = N_T/\pi r$ is the volume density at r in the equatorial plane [N_T is the sodium line of sight column content derived from the observed emission intensity ϵ in Rayleighs ($\epsilon = 0.48 \times 10^{-6} N_T$)] (*5*).
11. A. F. Cheng [*J. Geophys. Res.* **91**, 4524 (1986)] and D. D. Barbosa and A. Eviatar [*Astrophys. J.* **310**, 927 (1986)] were the first to discuss this nonradial velocity component that leads to the flaring angle.
12. Ion cooling is discussed by D. D. Barbosa, F. V. Coroniti, and A. Eviatar [*Astrophys. J.* **274**, 429 (1983)] and is reviewed recently by A. F. Cheng [*Adv. Space Res.* **12**, 353 (1992)].
13. As discussed in E. J. Smith, K.-P. Wenzel, and D. F. Page [*Science* **257**, 1503 (1992)], most of the Ulysses instruments were turned off during the period of torus passage in order to safeguard their use for the primary mission. Indications of lower plasma densities in the torus were obtained by the radio beacon experiment (M. K. Bird *et al.*, *ibid.*, p. 1531).
14. Ions created from a "magnetospheric neutral wind" by photo-ionization and their subsequent radial transport are discussed in A. Eviatar and D. D. Barbosa [*J. Geophys. Res.* **89**, 7393 (1984)] and D. D. Barbosa [*ibid.* **91**, 5605 (1986)].

15. We thank N. Schneider for coordination of the Jupiter Watch Campaign; E. Smith for providing Ulysses trajectory information; D. Nottingham for assisting in the observations and data analysis; and D. Barbosa for informative discussions. We thank the director and staff of the Mount Haleakala Observatory for their assistance. This work was funded, in part, by NASA grant NAGW-2679.

29 May 1992; accepted 31 July 1992

Hubble Space Telescope Imaging of the North Polar Aurora on Jupiter

J. Caldwell, B. Turgeon, X.-M. Hua

The first direct images of the Jovian aurora at ultraviolet wavelengths were obtained by the Hubble Space Telescope Faint Object Camera near the time of the Ulysses spacecraft encounter with Jupiter on 8 February 1992. The auroral oval is not uniformly luminous. It exhibits a brightness minimum in the vicinity of longitude 180°. In the few images available, the brightest part of the oval occurs in late afternoon Jovian time. The observed oval is not concentric with calculated ovals in the O_6 model of Connerney. The size of the oval is consistent with auroral particles on field lines with magnetic *L* parameter >8, indicating significant migration from Io, its torus, or both, if these are their origins.

An aurora is the visible interaction between a planet's magnetosphere and its atmosphere. Auroral observations provide information on planetary magnetic fields (and thus, planetary interiors), magnetospheric species, and atmospheric composition and dynamics. Previous ultraviolet (UV) observations of the Jovian aurora from spacecraft such as the International Ultraviolet Explorer (IUE) and the Voyagers were made with spectrographs with large apertures and permitted only indirect inferences of spatial characteristics. Ground-based infrared (IR) images have also been obtained, but they are somewhat degraded spatially by Earth's atmosphere. We present here UV images of the Jovian aurora obtained by the Hubble Space Telescope (HST) that reveal the auroral oval for the first time. The images generally confirm previous auroral observations and models of the Jovian magnetic field, with some significant exceptions.

The HST Faint Object Camera (FOC) obtained six images (Fig. 1) of the Jovian north polar aurora in the H_2 Lyman band near 160-nm wavelength. The images were taken in two groups of three (Table 1), respectively ~13 and 3 hours before the time of closest approach to Jupiter by the Ulysses spacecraft (*1, 2*).

The photometric properties of Jupiter enhance the observability of its aurora (*3*). Increased absorption of UV sunlight at the poles (Fig. 1) due to high-latitude, high-altitude aerosols provides a relatively dark background. If the background at the poles were as bright as at lower latitudes, auroral contrast would be greatly reduced.

Images 101, 102, and 201 have similar central meridian longitudes (CMLs) in System III (*4*) (~150°) and images 202 and 203 also have similar CMLs (~190°). In each H_2 image an auroral oval may be seen, with those at CML ~190° having more favorable orientations. For each case, the astronomically westernmost part of the oval (local Jovian evening) is the brightest, with a second brightness maximum at the easternmost position.

Limb brightening, which occurs in an optically thin emitting region, is not the primary determinant of the apparent brightness variations along the oval. First, it could not introduce the observed east-west

Space Astrophysics Laboratory, Institute for Space and Terrestrial Science, 2700 Steeles Avenue West, Suite 202, Concord, ON L4K 3C8, Canada.

asymmetry. Second, the two images at CML ~190° have western maxima well within the limb, whereas limb brightening produces maxima at the limb. And third, part of the oval near the CML in the latter two images is significantly more faint than other parts that are not much closer to the limb. Therefore, the oval is not uniformly bright along its arc.

The individual images in Fig. 1 are shown in false color to enhance the visibility of faint auroral features. This enhancement process distorts judgment of relative brightness made by the eye. Table 2 presents a quantitative summary of three of the images, 102, 202, and 203. The information in this table helps confirm the large relative brightness of the western part of the oval for images 202 and 203 (CML ~190°). This is consistent with an auroral model in which the brightest spot on the oval, while remaining approximately fixed in local time of day, is modulated by Jupiter's rotation so that the bright spot is brightest when the CML ~190°. This will be discussed below relative to auroral observations at other wavelengths.

Furthermore, the section of minimum brightness along the oval is relatively faint with respect to much of the surrounding area—that is, many regions within the oval and also many at lower latitudes are somewhat brighter than that section of the oval. The general increase in brightness toward the equator is also evident.

Polar projection gives an additional perspective of the aurora (Figs. 2 and 3). For two reasons, the entire sequence of images was scheduled so that the CML would be as close as possible to 180°. First, in the northern hemisphere the aurora was expected to extend to its maximum southward latitudes near 180° longitude, according to models. Second, thermal IR images at 8-μm and longer wavelengths have consistently shown a single, large bright spot at the position of 180° longitude, 60° north latitude (5).

The UV auroral oval does extend farthest south near 165° longitude, reaching 50°N latitude (Fig. 2). However, there is a relative brightness minimum on the oval, centered at 170° longitude, extending about ±15° from there. This UV brightness minimum includes the longitude of the 8-μm bright spot. Figure 2 also shows that the brightest part of the oval is at its astronomically western extremity, in the longitude range of 140° to 145°, 52°N latitude.

In the three images clustered near CML ~150° (Fig. 3), the auroral oval has the same size and orientation with respect to System III as the oval in Fig. 2. There is also a relative minimum brightness of the oval near 170° longitude indicating that the region of minimum UV brightness is approximately fixed in System III coordinates, much like the thermal IR bright spot (5). The CML of Fig. 3 differs from that of Fig. 2 by about 40°.

Unlike the constancy of the longitude of minimum brightness, however, the brightest spot on the oval has moved to 90° longitude, 75° latitude, in Fig. 3. It is still at the westernmost part of the oval but has moved in longitude by about the same amount that the CML has changed, remaining at the same local time of day.

A UV brightness minimum at longitude 170° ± 15° differs somewhat from the interpretation of UV observations by Livengood *et al.* (6). They analyzed IUE observations of the aurora from 1981 to 1991, from wavelengths of 156 to 162 nm, which corresponded closely to our wavelengths (Table 1) but did not overlap in time. One of their primary conclusions was that the northern aurora had a UV brightness maximum at ~194° longitude, with significant variability about this position. That is compatible with the

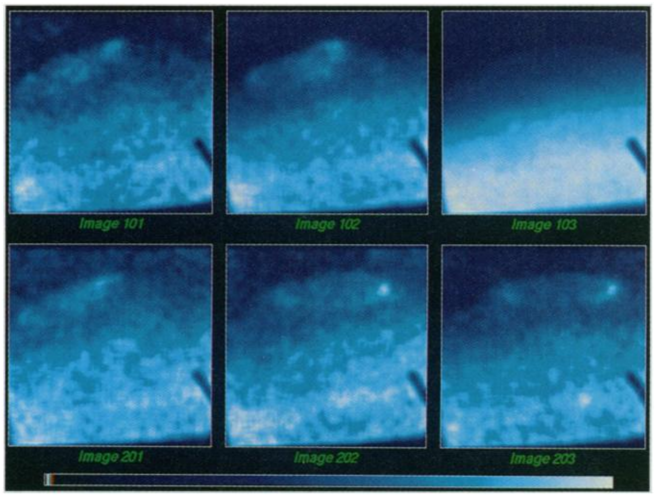

Fig. 1. Images of the Jovian aurora from the HST/FOC identified by the numbers from Table 1. An "occulting finger," planned for imaging faint regions near very bright stars, is visible in the mid-latitude background (lower right) of each image. Image 103, taken with different filters than were used with the others, shows the planetary limb unambiguously, spectrally excluding the auroral emissions.

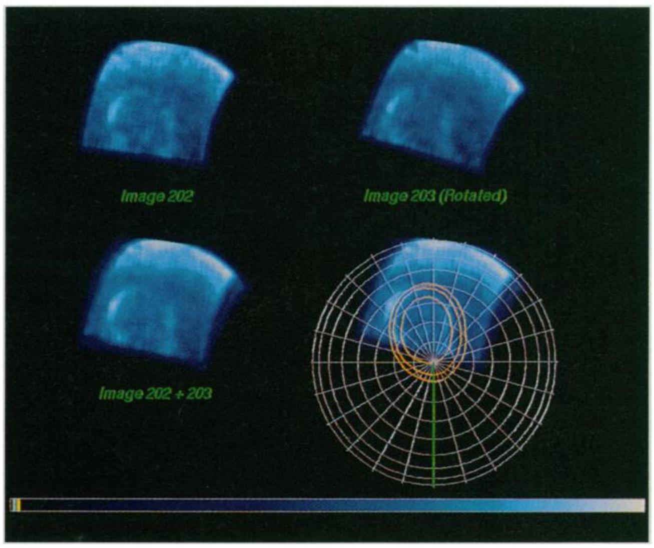

Fig. 2. Polar projections of two images, each with CML ~190°. Image 203 is rotated counterclockwise by 9° relative to the orientation of image 202 to compensate for planetary rotation. At the lower left a composite is shown; at the lower right the composite is repeated, with a latitude-longitude grid and model auroral ovals superimposed. The enhanced line projecting to the bottom of the grid corresponds to 0° longitude (System III). The earthward/sunward direction is perpendicular to the north polar terminator, which projects as a straight line approximately parallel to the 105 longitude/285 longitude great circle.

Table 1. Hubble Space Telescope UV imaging of the Jovian aurora.

Image	Time	Exposure time	Filters	CML (deg)
101	92.038/21:53:44	7 min	F140W, F152M	143
102	92.038/22:07:03	16 min	F140W, F152M	154
103	92.038/22:29:39	2.3 min	F175W, F170M	163
201	92.039/07:40:20	9 min	F140W, F152M	138
202	92.039/09:06:58	9 min	F140W, F152M	190
203	92.039/09:21:47	9 min	F140W, F152M	200

HST images, particularly because they represent an instantaneous snapshot and the IUE data show temporal variability.

Livengood *et al.* (6) recorded spectra in an aperture that was oval in shape with a long axis of 21.6 arc sec and a short axis of 8.9 arc sec. The IUE spatial resolution is more than 100 times worse than the HST pixel size after binning was completed. They investigated many possible models for the brightness distribution in their aperture but not the model suggested here—a fixed oval with a bright spot that is approximately fixed in local time of day, modulated by Jupiter's rotation. In fact, if they had done so, they would have violated Occam's razor.

We suggest that Livengood *et al.* (6) were detecting, in their large aperture, the increased brightening in the local evening part of the oval that occurs when the CML is ~180°. Because this area was close to the edge of their aperture, minor pointing errors in the IUE fine guiding system could account for some of their reported variability.

The size of the oval is important to determine the magnetospheric origin of the high-energy particles responsible for the aurora. In both Figs. 2 and 3 there are three computed ovals superimposed on the data. From the largest to the smallest, these correspond, respectively, to Jovian magnetic field lines crossing the Jovian equator at R_J (radius of Jupiter) = 6 and 8 and the last closed field line, according to the O_6 model of Connerney (7). The observed auroral oval had its long axis roughly parallel to the long axis of the computed model ovals, but it was slightly offset from the center of those ovals. Connerney (7) notes that a central position shift between the observed and the computed ovals does not mean the two are incompatible. However, the size of the observed oval is extremely significant. It was clearly larger than the oval corresponding to the last closed field line, consistent with the positioning on closed field lines of particles that excite the emission, as expected.

Further, the observed oval was distinctly smaller than the R_J = 6 and R_J = 8 ovals, which suggests that the auroral particles are on field lines well outside the orbit of Io. Assuming that Io was the origin of these particles, we conclude that they diffused radically outward from Io before being able to penetrate the atmosphere of Jupiter to auroral altitudes. The proximity of the auroral field lines to open lines may be responsible for the proposed time-of-day effect on the maximum auroral brightness region, because the open field lines are perturbed by Jupiter's rotation.

Finally, there were many similar aspects between our HST images and the near IR images of H_3^+ auroral emission observed at the NASA Infrared Telescope Facility (IRTF) (8, 9). The IRTF spatial resolution is much inferior to the HST resolution, but the IRTF images have much higher signal-to-noise ratios and there are many more IRTF images with which to work. For example, the images obtained by Kim *et al.* (9) of H_3^+ emission at 3.533 μm show extremely good morphological agreement with the HST images taken less than a month earlier.

For the north, Drossart *et al.* (8) report 1991 observations of two H_3^+ "auroral spots" separated by ~60° in longitude on either side of the central meridian, joined by a weaker arc of emission. The whole structure was centered at about longitude 180° with much weaker emission outside this range. Their description is quite consistent with our images.

Drossart *et al.* (8) report that auroral behavior is more complex in the south, for which no HST observations have yet been made, than in the north. From their numerous images they suggest that there is a bright spot on the southern auroral oval fixed approximately in local time and modulated by System III longitude. This finding has strongly influenced the hypothesis that a similar model applies to the north.

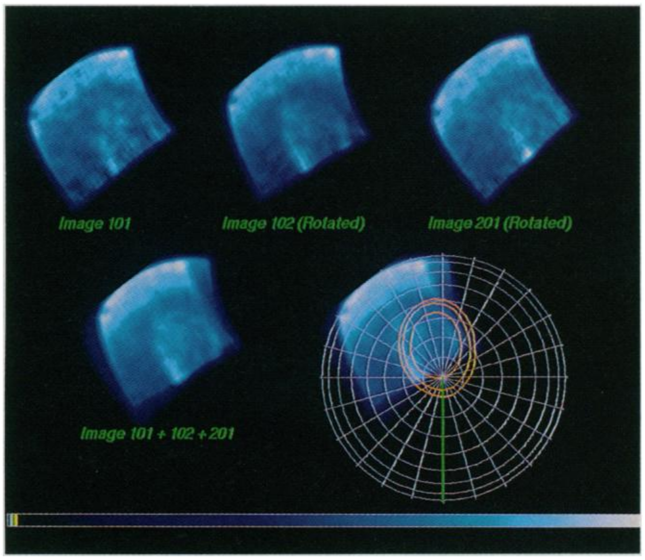

Fig. 3. Similar to Fig. 2 except for the three images with CML ~150°. Note that the oval remains fixed in System III coordinates, while the apparent direction to the sun/earth changes as Jupiter rotates.

Table 2. Photometry of selected regions (relative units).

Region	Image 102	Image 202	Image 203
Brightest area, western part of oval (*10*)	1.24 ± 0.26	1.59 ± 0.30	1.64 ± 0.30
Brightest area, eastern part of oval	1.02 ± 0.11	1.16 ± 0.25	1.19 ± 0.27
On oval, minimum brightness area	0.88 ± 0.13	0.98 ± 0.16	1.00 ± 0.24
Inside oval	0.97 ± 0.15	1.08 ± 0.15	0.93 ± 0.20
Below oval	1.24 ± 0.30	1.28 ± 0.18	1.24 ± 0.17
Mid-latitude	1.27 ± 0.33	1.51 ± 0.15	1.63 ± 0.19

REFERENCES AND NOTES

1. In each case, two filters were used in series in the FOC. This was done to suppress the overwhelming excess of visible wavelength photons from Jupiter, to which the FOC detectors are sensitive, with respect to UV photons. Typical FOC filters have peak transmissions of order 3 × 10^{-1} and long wavelength tails with transmissions of order to 10^{-3}. Because the transmissions are multiplicative, a pair of filters with spectrally near-coincident peaks has a high transmission of order 10^{-1} with a long wavelength tail transmission of order 10^{-6}. This is adequate to suppress the visible photons, which exceed the expected auroral flux (determined from independent observations by the IUE) by approximately four orders of magnitude. Five of the six images were obtained with the filter pair F140W, F152M. In this notation, the three-digit number gives the wavelength of peak transmission of an individual filter in nanometers, and W and M denote "wide" or "narrow" filters. The final image was taken with the filter pair F175W, F170M, which effectively excludes H_2 emission and achieves a significantly higher exposure level from the brighter continuum of reflected sunlight at longer wavelengths and in less time than does the F140W, F152M pair. The continuum image was used to verify the position of the limb of Jupiter to measure the zenographic position of auroral features most accurately.
2. The data have been flat-fielded, and cosmic ray hits on individual pixels have been removed. The FOC was used in its *f*/96 zoom mode, and the field of view was 22 by 22 arc sec². The original format was 512 by 1024 pixels, with each pixel being 0.044 by 0.022 arc sec². The images were subsequently rebinned to an effective resolution of 0.35 arc sec (full width at half maximum for a

point source) to improve the signal-to-noise ratio. Exposure times were calculated from IUE auroral spectra but depended on assumptions about the emission geometry in the large IUE aperture and so were initially quite inaccurate. A trade-off was necessary between longer exposure times to collect more photons and shorter ones to minimize the effect of Jupiter's rotation. A number of different exposure times were therefore tried, with the longer ones being more successful.

3. In images at longer wavelengths, selected to be in one of several strong absorption bands of methane (CH_4) such as 890 or 2200 nm wavelength, the polar caps of Jupiter are relatively brighter than the rest of the planet. The enhanced brightness is due to high-altitude particles that are relatively concentrated at the poles and that scatter sunlight before the CH_4 can absorb it. At other locations on Jupiter the CH_4 is an effective absorber. However, at the much shorter UV wavelengths of the HST images the particles are intrinsically strong absorbers and make the pole relatively darker than the rest of the planet. The darkening is zonal, not concentric with the subsolar point, which demonstrates independently of other considerations that it is due to latitudinally inhomogeneous composition and not to radiative transfer effects in a uniform atmosphere. The bottom of the images extends almost to the equator of Jupiter. It is not a coincidence that this effect occurs where it does on Jupiter. The source of the near IR–scattering/UV-reflecting particles is radiochemistry, induced by the influx of high-energy magnetospheric particles on Jupiter's atmosphere of H_2 and CH_4. When CH_4 is radiologically dissociated, the products polymerize to form the particles at the high latitudes where bombardment occurs.
4. System III is a longitudinal and rotational reference frame determined by the observed rotation rate (870.536° per day) of Jupiter's magnetosphere, which is identical to the rotation rate of the planetary interior. Two other atmospheric rotation rates are associated with Jupiter: System I (equatorial, 877.900° per day) and System II (high-latitude, 870.270° per day).
5. J. Caldwell, H. Halthore, G. Orton, J. Bergstralh, *Icarus* **74**, 331 (1988); J. Caldwell, A. T. Tonkunaga, G. S. Orton, *ibid.* **53**, 133 (1983).
6. T. A. Livengood, H. W. Moos, G. E. Ballester, R. M. Prangé, *ibid.* **97**, 26 (1992).
7. J. E. P. Connerney, in *Planetary Radio Emissions III*, H. Rucker and S. J. Bauer, Eds. (Austrian Academy of Sciences Press, Vienna, in press); ______, M. H. Acuna, N. F. Ness, in preparation.
8. P. Drossart, R. Prangé, J.-P. Maillard, *Icarus* **97**, 10 (1992); R. Baron *et al.*, *Nature* **353**, 539 (1991).
9. S. J. Kim, J. Caldwell, T. Herbst, in preparation.
10. The "brightest area, western or eastern part of the oval" refers to a single 5 by 5 box of the brightest pixels in those parts of the oval. The other areas refer to an average of ~20 such 5 by 5 boxes. For images 202 and 203, where the oval is tilted significantly earthward, the standard deviations are accordingly lower. For image 102, where the oval is not as favorably oriented, the standard deviations are irregular.
11. We thank J. E. P. Connerney for helpful private communications.

1 June 1992; accepted 5 August 1992

Magnetic Field Observations During the Ulysses Flyby of Jupiter

A. Balogh, M. K. Dougherty, R. J. Forsyth, D. J. Southwood, E. J. Smith, B. T. Tsurutani, N. Murphy, M. E. Burton

The Jovian flyby of the Ulysses spacecraft presented the opportunity to confirm and complement the findings of the four previous missions that investigated the structure and dynamics of the Jovian magnetosphere and magnetic field, as well as to explore for the first time the high-latitude dusk side of the magnetosphere and its boundary regions. In addition to confirming the general structure of the dayside magnetosphere, the Ulysses magnetic field measurements also showed that the importance of the current sheet dynamics extends well into the middle and outer magnetosphere. On the dusk side, the magnetic field is swept back significantly toward the magnetotail. The importance of current systems, both azimuthal and field-aligned, in determining the configuration of the field has been strongly highlighted by the Ulysses data. No significant changes have been found in the internal planetary field; however, the need to modify the external current densities with respect to previous observations on the inbound pass shows that Jovian magnetic and magnetospheric models are highly sensitive to both the intensity and the structure assumed for the current sheet and to any time dependence that may be assigned to these. The observations show that all boundaries and boundary layers in the magnetosphere have a very complex microstructure. Waves and wave-like structures were observed throughout the magnetosphere; these included the longest lasting mirror-mode wave trains observed in space.

The primary aim of the Ulysses mission is the exploration of interplanetary space out of the ecliptic plane, in particular over the poles of the sun. The requirement for rotating the orbital plane of the spacecraft to enable it to reach high solar latitudes has resulted in a unique Jovian flyby trajectory (*1*). Whereas the inbound portion of the orbit was close to the planet-sun line (similar to previous flybys), close to the planet the spacecraft reached higher latitudes than previous missions. The outbound orbit traversed the previously unvisited dusk sector, and the spacecraft exited the Jovian environment at high southern latitudes. We report on the observations made with the magnetometer (*2*) onboard Ulysses along this new flyby trajectory.

A. Balogh, M. K. Dougherty, R. J. Forsyth, D. J. Southwood, The Blackett Laboratory, Imperial College, London SW7 2BZ, United Kingdom.
E. J. Smith, B. T. Tsurutani, N. Murphy, M. E. Burton, Jet Propulsion Laboratory, Pasadena, CA 91109.

The magnetic field strength measured during the inbound and outbound passes of the flyby is shown in Fig. 1, A and B, respectively. We have marked three separate regions on the inbound pass that categorize the general nature of the field data. The categorizations match those suggested previously (*3, 4*) and are made on the basis of the field morphology. The field is much more regular in the inner and middle regions, and the dominant feature is the periodic depressions in field strength [first observed by Pioneer 10 (*5*)], detected about every 10 hours, produced by encounters with, or approaches to, the magnetodisk. The distinction between the inner and middle regions is that the field is primarily radial in the middle regime [beyond about 30 Jovian radii (R_J)] and is dominated by the planetary dipole in the region defined as the inner magnetosphere. The outer region of the magnetosphere is characterized by a very disturbed field with large changes in field strength, some of which can be attributed to brief exits from the magnetosphere back into the magnetosheath. Other large deviations resemble the current sheet crossings recorded closer in. The real distinction between the regions is that the field in the outer region is not mainly radial, but rather is directed predominantly parallel to the planetary dipole.

The bow shock was encountered inbound at a radial distance from the planet of 113 R_J at 17:33 universal time (UT) on 2 February 1992. The shock was encountered only once inbound and was a quasi-parallel shock; the normal angle of 36° to the field was calculated with the use of magnetic coplanarity. The magnetopause current sheet was first encountered at a distance of 110 R_J at 21:30 UT on the same day. Other instruments on Ulysses identified magnetospheric signatures only about an hour later, implying the existence of a thick boundary layer.

All inbound Jovian spacecraft flyby trajectories, including that of Ulysses, entered the magnetosphere in the late morning equatorial sector. The magnetosphere observed by Ulysses was much expanded in comparison to the Voyager and Pioneer 11 inbound passes. Pioneer 10 first detected the magnetopause at 98 R_J.

The briefness of the magnetosheath sojourn indicates that the magnetosphere had expanded substantially between the shock and the first encounter with the magnetopause. Our data, which show a weak magnetic field immediately before the bow shock, after the termination of a corotating interaction region by a reverse shock 4 hours previously, are consistent with this